



# On-the-fly sampling of temperature-dependent thermal neutron scattering data for Monte Carlo simulations



Andrew T. Pavlou, Wei Ji\*

Department of Mechanical, Aerospace and Nuclear Engineering, Rensselaer Polytechnic Institute, 110 8th Street, Troy, NY 12180, USA

## ARTICLE INFO

### Article history:

Received 23 February 2014

Accepted 22 April 2014

Available online 15 May 2014

### Keywords:

On-the-fly sampling

Thermal neutron scattering

$S(\alpha, \beta)$  data

Temperature dependence

Monte Carlo simulation

## ABSTRACT

Temperature can strongly affect the probabilities of certain neutron interactions (fission, capture, scattering, etc.) with materials. These probabilities are referred to in the nuclear community as ‘cross sections’ and are used as inputs for computer simulations. During the lifetime of a nuclear reactor, the core and its surrounding materials will experience a wide range of temperatures. To simulate the neutronic behavior in a realistic core, it is required to pre-store a large amount of cross section data to encompass the entire temperature range a neutron may experience. In recent years, methods have been developed to reduce data storage and obtain the cross section at the desired temperature ‘on-the-fly’ during radiation transport simulations using Monte Carlo codes. At thermal energies, however, the scattering of neutrons is complicated by their relatively small wavelengths, making molecular binding and lattice effects significant. Current approaches typically require nuclear data file sizes of tens to hundreds of MB per temperature, which can be prohibitive for realistic reactor physics simulations. To reduce the storage burden, a fitting approach in temperature is investigated that allows for the efficient evaluation of the thermal neutron scattering physics at an arbitrary temperature within a predefined range. The physics for thermal neutron scattering in graphite and hydrogen in water are evaluated with this approach. In both cases, the functional fits are able to accurately reproduce the scattering probabilities. The data storage for the fitting approach requires only a few 100 kB, which is a significant memory savings over the existing methods. These data can be used to sample a neutron’s outgoing energy and scattered angle at an arbitrary temperature with minimal errors.

© 2014 Elsevier Ltd. All rights reserved.

## 1. Introduction

### 1.1. On-the-fly sampling of nuclear data in Monte Carlo simulations

In reactor physics, nuclear reaction cross sections, as a function of neutron energy, are greatly affected by the temperature of the target material. One well-known phenomenon related to temperature effects is the Doppler broadening of cross sections at resonance neutron energies. The range of resonance energies can be broadened for fission and capture reactions as the material temperature increases due to the change in relative motion between the neutron and the target. In order to accurately model this phenomenon in the computer simulation of neutron transport and account for temperature feedback in coupled neutronic–thermal–hydraulic reactor analysis, nuclear cross sections need to be pre-calculated and stored at a wide range of temperatures. This strategy becomes ineffective as computer memory is a concern.

In certain reactor designs like the Very High Temperature Gas-Cooled Reactors (VHTR), the temperature variation can be very broad and very sharp during normal and transient operations (Yesilyurt et al., 2007). This requires a prohibitive amount of memory usage to store cross section data on fine temperature bins. It is desired to seek an alternative strategy to store and use the temperature-dependent cross section data.

On-the-fly sampling is one effective means for reducing data storage in computer simulations, specifically for Monte Carlo method-based simulations. Ideally, it is desired that cross section data for neutron-nucleus reactions for any type and at any temperature can be generated and used on-the-fly during the random walk process without introducing additional computational costs compared with the pre-storage strategy. In order to achieve this, one needs to have a comprehensive understanding of physical models developed for all the cross sections evaluated and used in the past and to develop physics-based fast sampling methods that are tailored specifically for incorporation of cross sections into Monte Carlo simulations. Over the past few decades, less attention has been paid to this research area. This situation, however, has

\* Corresponding author. Tel.: +1 (518) 276 6602; fax: +1 (518) 276 6025.

E-mail address: [jw2@rpi.edu](mailto:jw2@rpi.edu) (W. Ji).

changed over the past few years. Recently, a method has been developed and implemented into the Monte Carlo code MCNP6 (Goorley et al., 2012) to on-the-fly sample cross sections of any reaction type for the most important resonance absorber nuclides (Yesilyurt et al., 2012). By only storing zero temperature cross sections, the Doppler broadening of total, fission and capture cross sections can be accurately sampled for the desired temperature and for any incoming neutron energy during the random walk. The computational storage has been significantly reduced by eliminating the need to store cross sections at every temperature of interest and for each isotope. Meanwhile, a new stochastic method has been developed to account for the motion of target nuclei on-the-fly by only using zero temperature cross sections in Monte Carlo neutron transport simulations. The method is based on explicit treatment of the motion of target nuclei at collision sites and the use of rejection sampling techniques. It is shown to be capable of accurately modeling continuous temperature distributions and has been implemented in the Monte Carlo reactor physics code Serpent (Viitanen and Leppänen, 2012).

For elastic scattering reactions in the epithermal energy range, new methods for the on-the-fly Doppler broadening of the elastic scattering kernel have also been developed in recent years: the Doppler Broadening Rejection Correction (DBRC) method (Becker et al., 2009) and the Weight Correction Method (WCM) (Lee et al., 2009). These methods show better accuracy than the original Sampling of the Velocity of the Target nucleus (SVT) algorithm (Carter and Cashwell, 1975) to on-the-fly sample a neutron's outgoing energy and angle after a scattering reaction at epithermal energies. Both the DBRC method and WCM involve sampling parameters in the center-of-mass frame followed by a conversion of sampled parameters back to the laboratory frame. More recently, an alternative method has been developed to directly sample a neutron's outgoing parameters in the laboratory frame with similar accuracy to the DBRC method (Sunny and Martin, 2013) by on-the-fly generating the moments of the differential scattering probability density function (PDF) at any temperature. For other important temperature-dependent cross sections, such as for scattering reactions that need to account for both thermal agitation and chemical bond effects at thermal energies and reactions at unresolved resonance energies, on-the-fly sampling methods have not yet been developed (Brown et al., 2012). In this paper, the focus is the on-the-fly sampling of  $S(\alpha, \beta)$  data at thermal energies.

In previously developed on-the-fly sampling methods, the distribution of the target nuclide energy is assumed to follow a Maxwell–Boltzmann distribution. This assumption leads to the formation of analytical expressions as a function of energy and temperature for the previously studied cross sections or scattering kernel. Although these expressions are in complicated forms, such analytical temperature dependence allows the functional expansion of cross sections as a summation of a series of simple basis functions, thus providing a fast approach to generate temperature-dependent cross sections on-the-fly. However, complications arise in the thermal energy region for scattering reactions. First, the assumption of the target isotopes following a Maxwell–Boltzmann distribution is not valid. Second, neutron–nucleus scattering interactions become much more complicated than epithermal scattering and resonance reactions. Consequently, functions to account for all the physics included in the scattering event are in a complicated integral form and do not have an analytical temperature dependence (Koppel et al., 1967). This makes it much more challenging or even impossible to generate double differential scattering cross sections on-the-fly following similar methods developed for cross sections at resolved-resonance and epithermal energies. A new strategy is needed to treat the temperature dependence of the double differential scattering data in the thermal energy region. In this paper, we present an on-the-fly methodology

that can sample a neutron's outgoing energy and flight angle after a thermal scattering event at an arbitrary temperature. This method removes the need to store the inelastic double differential thermal scattering cross section data at discrete temperatures.

## 1.2. Thermal neutron scattering with nuclear materials

When thermal neutrons interact with bound isotopes, the atom's translational, rotational and vibrational motions, which are strongly correlated with the ambient temperature, can affect the neutron scattering cross sections as well as the outgoing energy and angle after the scatter. These effects are significant for neutrons in the thermal energy range ( $<4$  eV). In the thermal energy region, the neutron and target have comparable energies so that competing inelastic upscattering and downscattering events occur. In addition, the scattering process is divided into a coherent and an incoherent portion, where the incoherent portion ignores interference effects between the neutron and the target where the scattering from different planes of atoms can interfere as the neutron wavelength hits different atomic spacings. Both incoherent and coherent inelastic scattering are important for all moderating materials, though it is typical to ignore the coherent part of inelastic scattering with minimal error (MacFarlane et al., 2012). Therefore, the focus of this paper is on incoherent inelastic neutron scattering. Methods for temperature correcting the elastic portion of thermal neutron scattering are saved for future work.

The incoherent inelastic differential scattering cross section in the thermal region is denoted by Bischoff and Yeater (1972)

$$\sigma(E \rightarrow E', \Omega \cdot \Omega', T) = \frac{\sigma_b}{2kT} \sqrt{\frac{E'}{E}} e^{-\beta} S(\alpha, \beta, T), \quad (1)$$

where  $E$  and  $E'$  represent the pre- and post-collision energy, respectively,  $\Omega \cdot \Omega'$  represents the pre- and post-collision scattering angle ( $\Omega \cdot \Omega' = \mu$ , where  $\mu$  is the cosine of the scattering angle),  $\sigma_b$  is the bound atom scattering cross section,  $k$  is the Boltzmann constant ( $=8.617E-5$  eV/K),  $T$  is the ambient temperature and  $S(\alpha, \beta, T)$  is the symmetric form of the scattering law which contains much of the thermal scattering physics. The variables  $\alpha$  and  $\beta$  are dimensionless quantities that define momentum and energy transfer, respectively,

$$\alpha = \frac{E + E' - 2\mu\sqrt{EE'}}{A_0kT}, \quad (2)$$

$$\beta = \frac{E' - E}{kT}, \quad (3)$$

where  $A_0$  is the mass ratio of the target nucleus to neutron. In classical quantum mechanics, the scattering law is related to a dynamic structure factor (Sutton et al., 2009) by

$$S(\alpha, \beta) = e^{\beta} \frac{kT}{\hbar} S(\boldsymbol{\kappa}, \omega), \quad (4)$$

where  $\hbar\boldsymbol{\kappa}$  and  $\hbar\omega$  represent, respectively, momentum and energy transfer and  $S(\boldsymbol{\kappa}, \omega)$  is the dynamic structure factor. The dynamic structure factor is the time Fourier transform of the intermediate scattering function,  $\chi(\boldsymbol{\kappa}, t)$ ,

$$S(\boldsymbol{\kappa}, \omega) = \frac{1}{2\pi} \int e^{-i\omega t} \chi(\boldsymbol{\kappa}, t) dt, \quad (5)$$

while the intermediate scattering function is the spatial Fourier transform of a self-correlation function,  $G_s(\mathbf{r}, t)$ ,

$$\chi(\boldsymbol{\kappa}, t) = \int e^{i\boldsymbol{\kappa} \cdot \mathbf{r}} G_s(\mathbf{r}, t) d\mathbf{r}. \quad (6)$$

The differential self-correlation factor,  $G_s(\mathbf{r}, t) d\mathbf{r}$ , is the conditional probability of a nucleus located in  $d\mathbf{r}$  about  $\mathbf{r}$  at some time  $t$  given the same nucleus located at the origin at time zero. Approx-

imations can be applied to the self-correlation function for certain materials to make the calculation of the scattering law easier. However, in general, the scattering law  $S(\alpha, \beta, T)$  is a complicated function with no smooth temperature or energy dependence.

### 1.3. Thermal neutron scattering data storage in Monte Carlo codes

Scattering law data are generated in NJOY (MacFarlane et al., 2012) and stored in ENDF thermal scattering files for specific moderator materials on a mesh of alpha and beta values at specific temperatures. Interpolation laws are provided for each material to obtain intermediate values in the  $(\alpha, \beta)$  space within a specified fractional tolerance. Monte Carlo codes, e.g., Racer and MC21, use a method of obtaining data continuous in angle and energy (Ballinger, 1995; Sutton et al., 2007) and, in recent years, the traditional discrete-in-energy thermal neutron scattering treatment used in MCNP has been improved and tested to allow for a continuous-in-energy treatment (Pavlou et al., 2012). The continuous representation requires a fine energy mesh. To accurately model a system, the cross section data must encompass the entire energy and temperature ranges. The continuous  $S(\alpha, \beta, T)$  data sets, however, can be quite large even for a single temperature. Table 1 shows the continuous  $S(\alpha, \beta, T)$  file sizes in ENDF/B-VII.1 for selected moderator materials produced by NJOY at room temperature (MacFarlane et al., 2012).

The  $S(\alpha, \beta, T)$  datasets at many temperatures are often needed to model a realistic nuclear reactor system. For example, TRIGA research reactors are inherently safe because of the U-ZrH fuel used which gives a prompt negative temperature coefficient (Terrani et al., 2012). The operating temperature of the fuel ranges from about 300 K to 1000 K, so many  $S(\alpha, \beta, T)$  datasets are needed for H in ZrH to model a TRIGA reactor in the thermal energy region. One of the Generation IV reactor designs, the VHTR, is graphite-moderated and the operation temperature can exceed 1200 K. During accident scenarios like the Loss of Forced Cooling (LOFC), the maximum fuel temperature can reach around 2000 K under operation of the Reactor Core Cooling System (RCCS) (Vilim et al., 2004). In the safety analysis and evaluation, thermal scattering nuclear data including  $S(\alpha, \beta, T)$  datasets of graphite material in the temperature range from room temperature to the above temperatures are needed to provide reliable neutronic and thermal-hydraulic calculations for the normal, transient and accident scenarios.

In current Monte Carlo codes, tabulated values of the cumulative distribution functions (CDF) for alpha and beta based on  $S(\alpha, \beta, T)$  datasets are stored at different temperatures. Whenever a scattering reaction occurs in a region with a specified temperature, values of alpha and beta are sampled from the tabulated CDF values at the corresponding temperature. Linear interpolation is needed if sampled random numbers do not match the tabulated values. The neutron's outgoing energy and direction are then determined by the sampled alpha and beta using Eqs. (2) and (3). For our work, we develop an on-the-fly sampling method to obtain the outgoing parameters without storing any tabulated CDF values for alpha and beta at a temperature. The method is implemented

by examining the temperature dependences of alpha and beta at selected discrete values of the CDFs in alpha and beta. The functional temperature dependence is constructed through appropriate regression models that provide the best fitting to the actual temperature dependence based on  $S(\alpha, \beta, T)$  data generated by NJOY at a broad range of temperatures and incoming energies. Only fitting coefficients in the selected regression model need to be stored for Monte Carlo codes, eliminating the need to store continuous  $S(\alpha, \beta, T)$  datasets at all temperatures. These fitting coefficients would be used to sample alpha and beta (and thus scattered energy and scattering angle) at any temperature on-the-fly. In this method, the key step is to find accurate models for alpha and beta values as a function of temperature at equally-probable sampled CDF values for all temperatures.

In the next section, the method of constructing the PDF/CDF forms of alpha and beta that can be used to sample the scattered neutron energy and angle of scatter at a single temperature is first introduced. Then, these CDF forms at different temperatures and different incoming energies are investigated for generally-used light material nuclei. The temperature dependence of these CDFs will be determined by fitting to several regression models. The final functional form for the temperature dependence of alpha and beta at different values of CDFs will be constructed based on the best fitted regression model. On-the-fly sampling of the outgoing parameters can be implemented using the obtained functional forms.

## 2. Construction of PDFs/CDFs in alpha and beta based on thermal scattering nuclear data

The procedure to construct alpha and beta PDFs/CDFs is based on the direct sampling method used by Ballinger when he studied thermal neutron scattering data (Ballinger, 1995). The construction is performed by first converting the double differential cross section from a function of  $E \rightarrow E', \mu, T$  to a function of  $\alpha, \beta, T$ . This is done through a Jacobian transformation,

$$\frac{\sigma(E \rightarrow E', \mu, T)}{\sigma(\alpha, \beta, T)} = \det \begin{vmatrix} d\alpha/dE & d\alpha/d\mu \\ d\beta/dE & d\beta/d\mu \end{vmatrix}. \quad (7)$$

The determinant of the Jacobian is readily found to be

$$\det \begin{vmatrix} d\alpha/dE & d\alpha/d\mu \\ d\beta/dE & d\beta/d\mu \end{vmatrix} = \frac{2\sqrt{EE'}}{A_0(kT)^2}. \quad (8)$$

Combining Eqs. (1), (7), and (8) gives

$$\sigma(\alpha, \beta, T) = \frac{\sigma_b A_0 kT}{4E} e^{-\frac{\beta}{2} S(\alpha, \beta, T)}. \quad (9)$$

In order to sample alpha and beta values based on Eq. (9) in the Monte Carlo code, a joint probability density function of alpha and beta should be constructed first. Dividing Eq. (9) by a total cross section, defined as the integration of Eq. (9) over all alpha and beta values, one obtains

$$f(\alpha, \beta|E, T) = \frac{\sigma(\alpha, \beta, T)}{\int_{\beta_{\min}}^{\beta_{\max}} \int_{\alpha_{\min}}^{\alpha_{\max}} \sigma(\alpha, \beta, T) d\alpha d\beta}. \quad (10)$$

The subscripts “min” and “max” correspond to minimum and maximum values, respectively. The alpha and beta bounds are determined using Eqs. (2) and (3). The minimum value of beta occurs for a scattered neutron with zero scattered energy. Thus,  $\beta_{\min} = -E/kT$ . In theory, the neutron can be upscattered to an infinite secondary energy. When a neutron interacts with a vibrating moderator atom, the positive momentum transfer that can occur has no theoretical limit. The upper limit is material-dependent and is usually chosen to increase until the CDF equals unity within

**Table 1**  
ENDF/B-VII.1 Continuous  $S(\alpha, \beta, T)$  file sizes for selected moderator materials at room temperature.

Material	File size [MB]
Graphite	24
Water	24.9
U in UO <sub>2</sub>	50
O <sub>2</sub> in UO <sub>2</sub>	75
Zr in ZrH	56
H in ZrH	116

some tolerance. In reality, it is unlikely the energy transfer will exceed 20 kT. Therefore,  $\beta_{\max} = 20$  is used in this work for both graphite and water. Similarly, the alpha bounds are calculated using the minimum and maximum angles of scatter. Thus,  $\alpha_{\min}$  and  $\alpha_{\max}$  are calculated by setting  $\mu$  equal to 1 and  $-1$  in Eq. (3), respectively,

$$\alpha_{\min} = \frac{(\sqrt{E} - \sqrt{E + \beta kT})^2}{A_0 kT}, \quad (11)$$

$$\alpha_{\max} = \frac{(\sqrt{E} + \sqrt{E + \beta kT})^2}{A_0 kT}, \quad (12)$$

In Eqs. (11) and (12), the quantity  $E + \beta kT$  comes from solving Eq. (3) for  $E'$ . Next, Eqs. (9) and (10) are combined to obtain

$$f(\alpha, \beta|E, T) = \frac{e^{-\frac{\beta}{2}S(\alpha, \beta, T)}}{\int_{\beta_{\min}}^{\beta_{\max}} \int_{\alpha_{\min}}^{\alpha_{\max}} e^{-\frac{\beta}{2}S(\alpha, \beta, T)} d\alpha d\beta} \quad (13)$$

This PDF is then broken up into two PDFs: one is a PDF in beta and the other is a conditional PDF in alpha given beta,

$$g(\beta|E, T) = e^{-\frac{\beta}{2}} \frac{\int_{\alpha_{\min}}^{\alpha_{\max}} S(\alpha, \beta, T) d\alpha}{\int_{\beta_{\min}}^{\beta_{\max}} \int_{\alpha_{\min}}^{\alpha_{\max}} e^{-\frac{\beta}{2}S(\alpha, \beta, T)} d\alpha d\beta}, \quad (14)$$

$$h(\alpha|\beta, E, T) = \frac{S(\alpha, \beta, T)}{\int_{\alpha_{\min}}^{\alpha_{\max}} S(\alpha, \beta, T) d\alpha}. \quad (15)$$

Integrating Eqs. (14) and (15) over beta and alpha, respectively, we obtain the CDFs in beta and alpha,

$$G(\beta|E, T) = \int_{\beta_{\min}}^{\beta} g(\beta'|E, T) d\beta', \quad (16)$$

$$H(\alpha|\beta, E, T) = \int_{\alpha_{\min}}^{\alpha} h(\alpha'|\beta, E, T) d\alpha'. \quad (17)$$

From Eq. (16), we see the beta CDF is dependent on two variables: the target temperature and the incoming neutron energy. The alpha CDF, however, is dependent on three variables: the target temperature, the incoming neutron energy and the energy transfer (beta). Because of this extra variable dependence in the alpha CDF, the storage of the alpha CDF data is quite large. However, because beta is a function of the incoming neutron energy, it is repetitive to store the alpha CDF data on both an incoming energy mesh and a beta mesh. Alternatively, for each beta, the alpha CDF can be stored over the entire alpha mesh (instead of

between the alpha bounds as calculated from the incoming neutron energy), thus removing the incoming energy dependence. This energy-independent alpha PDF is given by

$$\hat{h}(\alpha|\beta, T) = \frac{S(\alpha, \beta, T)}{\int_0^{\alpha_{\infty}} S(\alpha, \beta, T) d\alpha}, \quad (18)$$

where  $\alpha_{\infty}$  is the highest value in the alpha mesh. Eq. (18) is integrated over alpha to obtain its CDF,

$$\hat{H}(\alpha|\beta, T) = \int_0^{\alpha} \hat{h}(\alpha'|\beta, T) d\alpha'. \quad (19)$$

Eq. (17) is rewritten in terms of Eq. (19) as

$$H(\alpha|\beta, E, T) = \frac{\hat{H}(\alpha|\beta, T) - \hat{H}(\alpha_{\min}|\beta, T)}{\hat{H}(\alpha_{\max}|\beta, T) - \hat{H}(\alpha_{\min}|\beta, T)} \quad (20)$$

Eq. (20) shows that the alpha CDF data can be obtained by storing the energy-independent alpha CDF over the entire alpha mesh and then choosing the appropriate portion of the data based on the desired incoming neutron energy.

The procedure for sampling beta and alpha is:

- (1) For the desired incoming neutron energy and temperature, the beta bounds are calculated as previously described. This establishes the range of relevant beta values that are used in the  $S(\alpha, \beta, T)$  data for that material. The alpha bounds are calculated from Eqs. (11) and (12) for the incoming neutron energy and each beta value in its mesh. The CDF is constructed from Eq. (16).
- (2) A uniform pseudorandom number  $\xi$  is sampled in  $[0, 1]$  and set equal to the beta CDF, Eq. (16):  $\xi = G(\beta|E, T)$ . The CDF table is then searched for the random number and the sampled beta is given by  $\beta(T) = G^{-1}(\xi|E, T)$ .
- (3) For the incoming neutron energy, temperature and the beta that was just sampled, the alpha bounds are calculated from Eqs. (11) and (12). The CDF is constructed from Eq. (19).
- (4)  $\hat{H}(\alpha_{\min}|\beta, T)$  and  $\hat{H}(\alpha_{\max}|\beta, T)$  are then calculated. A second random number  $\zeta$  is sampled in  $[0, 1]$  and set equal to the alpha CDF, Eq. (17):  $\zeta = H(\alpha|\beta, E, T)$ . Eq. (20) is solved for  $\hat{H}(\alpha|\beta, T)$  to determine a new random number,  $\zeta'$ :

$$\hat{H}(\alpha|\beta, T) = \zeta \left[ \hat{H}(\alpha_{\max}|\beta, T) - \hat{H}(\alpha_{\min}|\beta, T) \right] + \hat{H}(\alpha_{\min}|\beta, T) = \zeta'. \quad (21)$$

The CDF table is searched for  $\zeta'$  and the sampled alpha is given by  $\alpha(T) = \hat{H}^{-1}(\zeta'|\beta, T)$ .

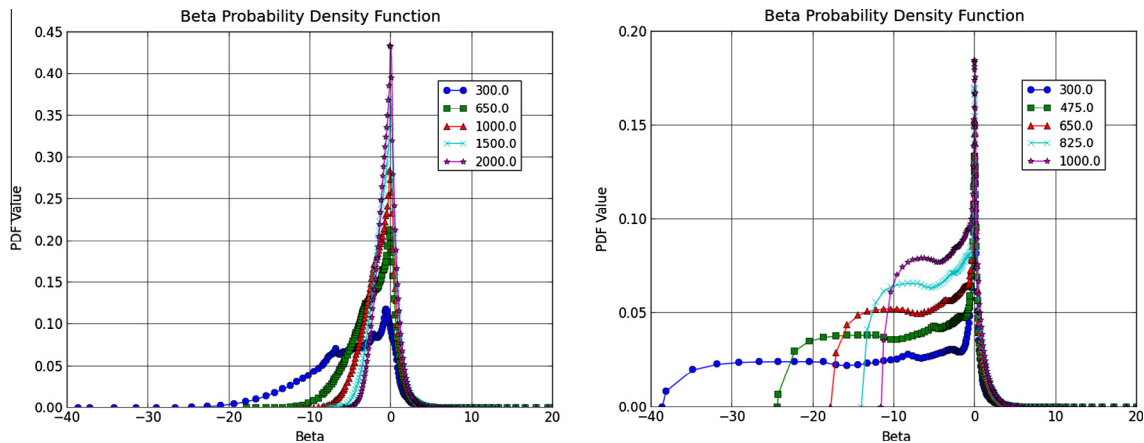


Fig. 1. Beta PDF for graphite (left) and H in H<sub>2</sub>O (right) at  $E_m = 1$  eV for various temperatures.

Fig. 1 shows an example of the beta PDF for graphite (left) and H in H<sub>2</sub>O (right) at  $E_{in} = 1$  eV for various temperatures. Fig. 2 shows an example of the alpha PDF for graphite (left) and H in H<sub>2</sub>O (right) at  $\beta = 10$  for various temperatures. The beta and alpha meshes were taken from the NJOY version 2012 user manual (MacFarlane et al., 2012) based on the original General Atomics evaluation.

Since the incoming energy is fixed to produce the beta PDF plots shown in Fig. 1, negative values of beta represent neutron downscattering events while positive values of beta represent upscattering events. As temperature increases, the fraction of downscattering at a fixed incoming energy slightly decreases. This is a result of the atoms being more energetic and allowing more energy to be transferred to the neutron.

In principle, after a thermal neutron scatters inelastically off an isotope, based on the incoming energy and the material temperature, one can sample the outgoing energy and scattered angle based on Eqs. (16) and (19). This is done by first sampling a value of beta from Eq. (16) and then sampling a value of alpha from Eq. (19). From alpha and beta, the scattered energy  $E'$  and cosine of the scattering angle  $\mu$  can be calculated from Eqs. (2) and (3),

$$E'_s = E + \beta_s kT, \tag{22}$$

$$\mu_s = \frac{E + E'_s - \alpha_s A_0 kT}{\sqrt{EE'_s}}, \tag{23}$$

where the subscript “s” indicates a sampled value. In practice, tabulated data are used for sampling beta and alpha. Eqs. (16) and (19) are the functional forms that one uses to tabulate values of beta and alpha at discrete CDF values. The tabular form can be easily utilized in Monte Carlo codes. The tabulation is performed at each incoming energy value and at each temperature for the beta CDF table. Similarly, the tabulation is performed at each beta value and at each temperature for the alpha CDF table. Such a format of data storage results in high computer memory usage if the range of temperature variation in a physical problem is too broad. These tabulated data can be expressed in the following form

$$G_i(\beta_j|E_k, T_l) \text{ and } \hat{H}_j(\alpha_j|\beta_i, T_l) \tag{24}$$

$$i = 1, 2, \dots, I$$

$$j = 1, 2, \dots, J$$

$$k = 1, 2, \dots, K$$

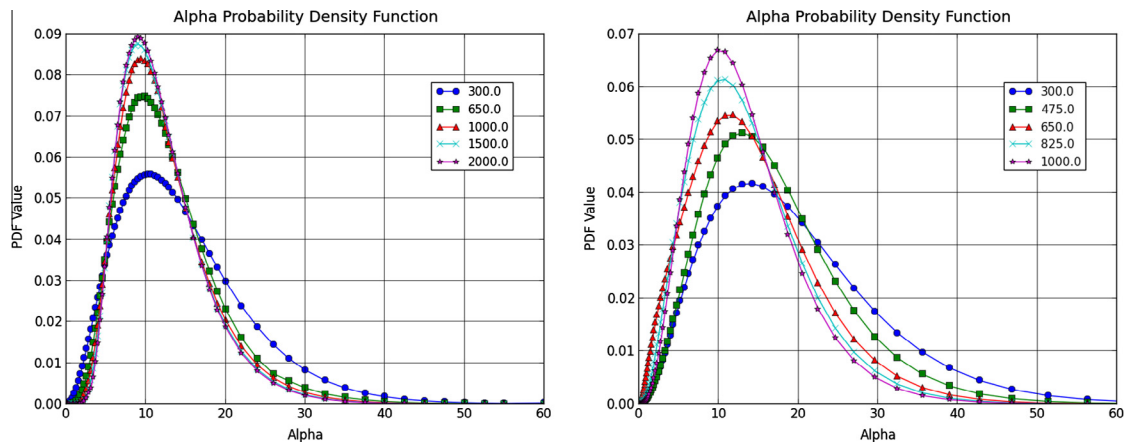


Fig. 2. Alpha PDF for graphite (left) and H in H<sub>2</sub>O (right) at  $\beta = 10$  for various temperatures.

Table 2  
Mesh values for CDF-dependent parameters for graphite.

Parameter	# of Mesh points	Mesh values
Incoming energy, $E_{in}$ [eV]	106	1.00E-5, 1.78E-5, 2.50E-5, 3.50E-5, 5.00E-5, 7.00E-5, 1.00E-4, 1.26E-4, 2.00E-4, 2.53E-4, 2.97E-4, 3.50E-4, 4.20E-4, 5.06E-4, 6.15E-4, 7.50E-4, 8.70E-4, 1.01E-3, 1.23E-3, 1.50E-3, 1.80E-3, 2.03E-3, 2.28E-3, 2.60E-3, 3.00E-3, 3.50E-3, 4.05E-3, 4.50E-3, 5.00E-3, 5.60E-3, 6.33E-3, 7.20E-3, 8.10E-3, 9.11E-3, 1.00E-2, 1.06E-2, 1.15E-2, 1.24E-2, 1.33E-2, 1.42E-2, 1.50E-2, 1.62E-2, 1.82E-2, 1.99E-2, 2.05E-2, 2.15E-2, 2.28E-2, 2.53E-2, 2.80E-2, 3.06E-2, 3.38E-2, 3.65E-2, 3.95E-2, 4.28E-2, 4.65E-2, 5.00E-2, 5.69E-2, 6.25E-2, 6.90E-2, 7.50E-2, 8.20E-2, 9.00E-2, 9.60E-2, 1.04E-1, 1.12E-1, 1.20E-1, 1.28E-1, 1.36E-1, 1.46E-1, 1.60E-1, 1.72E-1, 1.84E-1, 2.00E-1, 2.28E-1, 2.51E-1, 2.71E-1, 2.91E-1, 3.01E-1, 3.21E-1, 3.58E-1, 3.90E-1, 4.17E-1, 4.50E-1, 5.03E-1, 5.60E-1, 6.25E-1, 7.00E-1, 7.80E-1, 8.60E-1, 9.50E-1, 1.05, 1.16, 1.28, 1.42, 1.55, 1.70, 1.855, 2.02, 2.18, 2.36, 2.59, 2.855, 3.12, 3.42, 3.75
Energy transfer, $\beta$	96	0, 0.10081, 0.20162, 0.30244, 0.40325, 0.50406, 0.60487, 0.70568, 0.8065, 0.90731, 1.0081, 1.1089, 1.2097, 1.3106, 1.4114, 1.5122, 1.613, 1.7138, 1.8146, 1.9154, 2.0162, 2.117, 2.2179, 2.3187, 2.4195, 2.5203, 2.6211, 2.7219, 2.8227, 2.9235, 3.0244, 3.1252, 3.226, 3.3268, 3.4276, 3.5284, 3.6292, 3.73, 3.8308, 3.9317, 4.0325, 4.1333, 4.2438, 4.3648, 4.4976, 4.6431, 4.8025, 4.9772, 5.1687, 5.3786, 5.6087, 5.7347, 5.8608, 5.999, 6.1371, 6.2885, 6.44, 6.6059, 6.7718, 6.9538, 7.1357, 7.335, 7.5344, 7.7529, 7.9714, 8.2109, 8.4504, 8.9753, 9.5505, 10.181, 10.873, 11.63, 12.459, 13.37, 14.367, 15.46, 16.657, 17.97, 19.409, 20.986, 22.714, 24.608, 26.685, 28.96, 31.453, 34.187, 37.182, 40.466, 45, 50, 55, 60, 65, 70, 75, 80
Temperature, $T$ [K]	69	300, 325, 350, 375, 400, 425, 450, 475, 500, 525, 550, 575, 600, 625, 650, 675, 700, 725, 750, 775, 800, 825, 850, 875, 900, 925, 950, 975, 1000, 1025, 1050, 1075, 1100, 1125, 1150, 1175, 1200, 1225, 1250, 1275, 1300, 1325, 1350, 1375, 1400, 1425, 1450, 1475, 1500, 1525, 1550, 1575, 1600, 1625, 1650, 1675, 1700, 1725, 1750, 1775, 1800, 1825, 1850, 1875, 1900, 1925, 1950, 1975, 2000
CDF Probability	39	0.025, 0.05, 0.075, 0.1, 0.125, 0.15, 0.175, 0.2, 0.225, 0.25, 0.275, 0.3, 0.325, 0.35, 0.375, 0.4, 0.425, 0.45, 0.475, 0.5, 0.525, 0.55, 0.575, 0.6, 0.625, 0.65, 0.675, 0.7, 0.725, 0.75, 0.775, 0.8, 0.825, 0.85, 0.875, 0.9, 0.925, 0.95, 0.975

**Table 3**  
Mesh values for CDF-dependent parameters for water.

Parameter	# of Mesh points	Mesh values
Incoming energy, $E_{in}$ [eV]	95	1.00E-5, 1.78E-5, 2.50E-5, 3.50E-5, 5.0E-5, 7.00E-5, 1.00E-4, 1.26E-4, 2.00E-4, 2.53E-4, 2.97E-4, 3.50E-4, 4.20E-4, 5.06E-4, 6.15E-5, 7.50E-4, 8.70E-4, 1.01E-3, 1.23E-3, 1.50E-3, 1.80E-3, 2.03E-3, 2.28E-3, 2.60E-3, 3.00E-3, 3.50E-3, 4.05E-3, 4.50E-3, 5.00E-3, 5.60E-3, 6.33E-3, 7.20E-3, 8.10E-3, 9.11E-3, 1.00E-2, 1.06E-2, 1.15E-2, 1.24E-2, 1.33E-2, 1.42E-2, 1.50E-2, 1.62E-2, 1.82E-2, 1.99E-2, 2.05E-2, 2.15E-2, 2.28E-2, 2.53E-2, 2.80E-2, 3.06E-2, 3.38E-2, 3.65E-2, 3.95E-2, 4.28E-2, 4.65E-2, 5.00E-2, 5.69E-2, 6.25E-2, 6.90E-2, 7.50E-2, 8.20E-2, 9.00E-2, 9.60E-2, 1.04E-1, 1.12E-1, 1.20E-1, 1.28E-1, 1.36E-1, 1.46E-1, 1.60E-1, 1.72E-1, 1.84E-1, 2.00E-1, 2.28E-1, 2.51E-1, 2.71E-1, 2.91E-1, 3.01E-1, 3.21E-1, 3.58E-1, 3.90E-1, 4.17E-1, 4.50E-1, 5.03E-1, 5.60E-1, 6.25E-1, 7.00E-1, 7.80E-1, 8.60E-1, 9.50E-1, 1.05, 1.16, 1.28, 1.42, 1.55
Energy transfer, $\beta$	95	0, 0.006375, 0.01275, 0.0255, 0.03825, 0.051, 0.06575, 0.0806495, 0.120974, 0.161299, 0.241949, 0.322598, 0.403248, 0.483897, 0.564547, 0.645197, 0.725846, 0.806496, 0.887145, 0.967795, 1.04844, 1.12909, 1.20974, 1.29039, 1.37104, 1.45169, 1.53234, 1.61299, 1.69364, 1.77429, 1.85494, 1.93559, 2.01624, 2.09689, 2.17754, 2.25819, 2.33884, 2.41949, 2.50014, 2.58079, 2.6695, 2.76709, 2.87445, 2.9925, 3.12235, 3.2653, 3.42247, 3.59536, 3.78549, 3.99467, 4.22473, 4.47787, 4.75631, 5.06258, 5.39939, 5.76997, 6.17766, 6.62607, 7.11924, 7.66181, 8.25862, 8.91511, 9.63722, 10.432, 11.3051, 12.2668, 13.3243, 14.4867, 15.766, 17.1733, 18.7218, 20.4245, 22.2976, 24.3572, 26.6234, 29.1165, 31.8586, 34.8759, 38.1936, 41.844, 45.8583, 50.2749, 55.1331, 60.4771, 66.3554, 72.8215, 79.9338, 90, 100, 110, 120, 130, 140, 150, 160
Temperature, $T$ [K]	71	300, 310, 320, 330, 340, 350, 360, 370, 380, 390, 400, 410, 420, 430, 440, 450, 460, 470, 480, 490, 500, 510, 520, 530, 540, 550, 560, 570, 580, 590, 600, 610, 620, 630, 640, 650, 660, 670, 680, 690, 700, 710, 720, 730, 740, 750, 760, 770, 780, 790, 800, 810, 820, 830, 840, 850, 860, 870, 880, 890, 900, 910, 920, 930, 940, 950, 960, 970, 980, 990, 1000
CDF Probability	39	0.025, 0.05, 0.075, 0.1, 0.125, 0.15, 0.175, 0.2, 0.225, 0.25, 0.275, 0.3, 0.325, 0.35, 0.375, 0.4, 0.425, 0.45, 0.475, 0.5, 0.525, 0.55, 0.575, 0.6, 0.625, 0.65, 0.675, 0.7, 0.725, 0.75, 0.775, 0.8, 0.825, 0.85, 0.875, 0.9, 0.925, 0.95, 0.975

$$l = 1, 2, \dots, L.$$

Both discrete CDF sets in alpha and beta are temperature dependent and a total of  $L$  sets of tables are needed.  $L$  can be very large if the temperature variation is very sharp and the range of the variation is large in the analyzed problems. To reduce the memory requirement and to provide more convenient usage for Monte Carlo codes, we propose a different data storage format that Monte Carlo codes can easily implement on-the-fly to sample outgoing energy and angle at any temperature as needed. The idea is to remove the  $T_i$  mesh dependence for  $G$  and  $\hat{H}$  in Eq. (23) and instead move the temperature dependence to beta and alpha at each value of  $G$  and  $\hat{H}$ . Specifically, the new format is

$$G_i(\beta(T)|E_k) \text{ and } \hat{H}_j(\alpha_j(T)|\beta_i) \quad (25)$$

$$i = 1, 2, \dots, I$$

$$j = 1, 2, \dots, J$$

$$k = 1, 2, \dots, K.$$

If an accurate functional expansion in  $T$  for beta and alpha can be found at discrete values of  $G$  and  $\hat{H}$ , the storage of the data sets can be greatly decreased as long as the order of the function is

much smaller than  $L$ . We will first investigate the temperature dependence of alpha and beta based on the actual library data. Then, we will study the functional fitting of these dependencies.

### 3. Analysis of temperature dependence of alpha and beta CDFs

The temperature dependence of the beta CDF was examined at discrete CDF probability lines in the range  $[0, 1]$  and on a mesh of incoming neutron energies in the thermal range. In total, there were four variables considered in the analysis:  $E_{in}$ ,  $\beta$ ,  $T$  and  $P_\beta$ , where  $P_\beta$  is the beta CDF probability. Likewise, the temperature dependence of the alpha CDF was examined at discrete CDF probability lines and on a mesh of beta values. The alpha CDF temperature analysis consists of four variables:  $\beta$ ,  $\alpha$ ,  $T$  and  $P_\alpha$ , where  $P_\alpha$  is the alpha CDF probability.

To examine the temperature dependences of the beta CDF, uniform meshes of  $E_{in}$  and  $P_\beta$  are chosen. Likewise, the temperature dependence of the alpha CDF is examined on uniform beta and  $P_\alpha$  meshes. Tables 2 and 3 detail the meshes used for the CDF temperature dependence for graphite and water, respectively.

In ENDF/B-VII.1, the incoming energy mesh for both graphite and H in  $H_2O$  contains 116 values in the range  $[1E-5, 9.15]$  eV. In this study, the maximum energy used from this original mesh is determined from the maximum value of beta in the beta mesh (where  $E_{max} = \beta kT$  and  $T$  is room temperature). A total of 96 beta

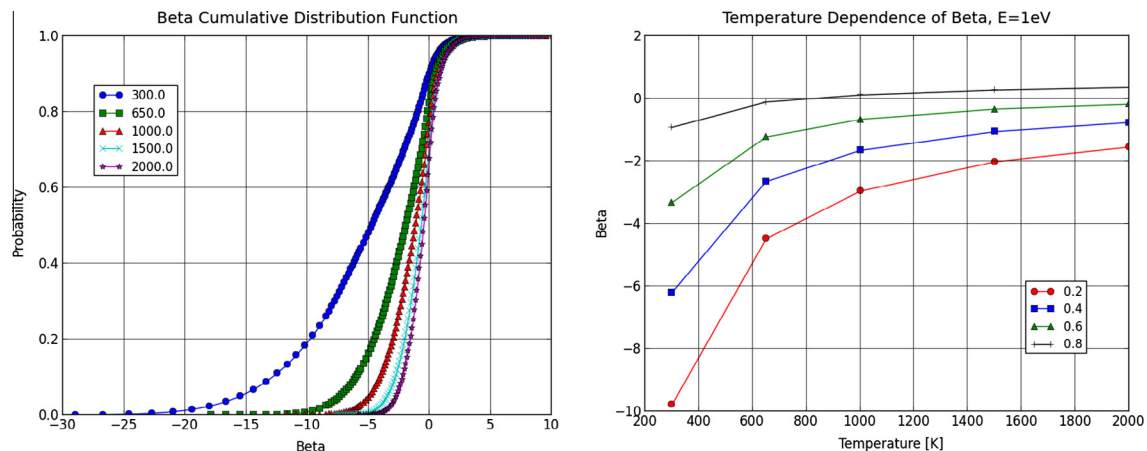


**Fig. 3.** Temperature dependence of beta CDF for graphite for  $E_{in} = 1$  eV.

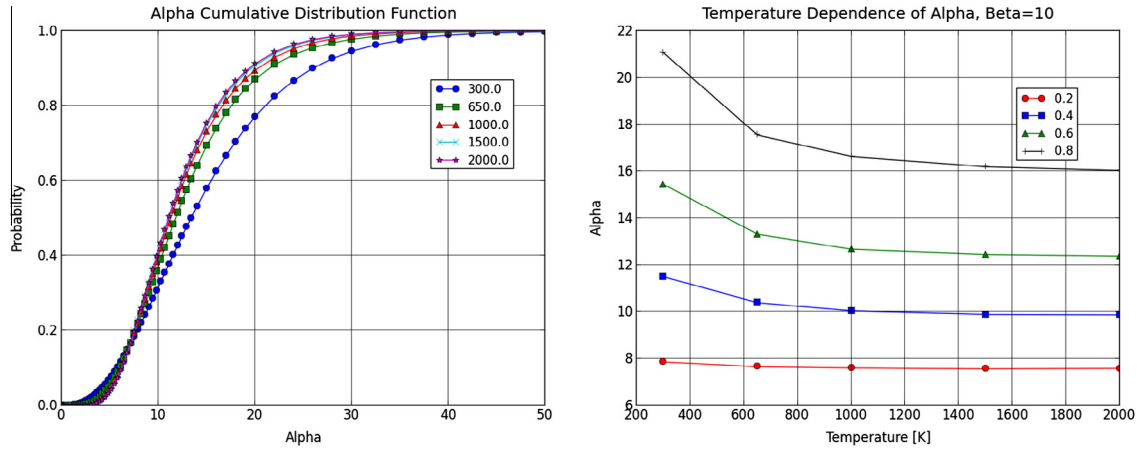


Fig. 4. Temperature dependence of alpha CDF for graphite for  $\beta = 10$ .

values are chosen in the range [0,80] for graphite and 95 beta values in the range [0,160] for H in H<sub>2</sub>O, consistent with the meshes ENDF (CSEWG and ENDF-6 Formats Manual, Broo, 2011) uses for graphite and H in H<sub>2</sub>O. Only positive values of beta are stored since  $S(\alpha, \beta, T)$  is symmetric about beta for both graphite and H in H<sub>2</sub>O. For both the beta and alpha CDFs for both moderators, 39 CDF probability lines in the range [0,1] are chosen.

Functional expansions based on different regression models are examined to fit the  $\beta(T)$  and  $\alpha(T)$  data at different values of alpha and beta CDFs. Based on the meshes described in the previous paragraph, the total number of fitting coefficients that needs to be stored for  $\beta(T)$  and  $\alpha(T)$  are, respectively,

$$N_{\beta} = \begin{cases} 106 \times 39 \times (n + 1) = 4134(n + 1) & \text{for graphite} \\ 95 \times 39 \times (n + 1) = 3705(n + 1) & \text{for H in H}_2\text{O} \end{cases} \quad (26)$$

$$N_{\alpha} = \begin{cases} 96 \times 39 \times (m + 1) = 3744(m + 1) & \text{for graphite} \\ 95 \times 39 \times (m + 1) = 3705(m + 1) & \text{for H in H}_2\text{O} \end{cases} \quad (27)$$

Table 4  
Fits for  $\beta(T)$  and  $\alpha(T)$  analysis.

Fit number	Fit	Fit number	Fit
1	$\sum_{n=0}^N a_n T^n$	5	$\sum_{n=0}^N a_n (\ln T)^n$
2	$\sum_{n=0}^N a_n T^{-n}$	6	$\sum_{n=0}^N a_n (\ln T)^{-n}$
3	$\sum_{n=0}^N a_n (\sqrt{T})^n$	7	$\sum_{n=0}^N a_n (\sqrt{\ln T})^n$
4	$\sum_{n=0}^N a_n (\sqrt{T})^{-n}$	8	$\sum_{n=0}^N a_n (\sqrt{\ln T})^{-n}$

where n and m are the order of the functional expansion for the  $\beta(T)$  and  $\alpha(T)$  fits, respectively.

The temperature dependence was performed on a temperature mesh of 69 values in the range [300,2000] K at 25 K increments for graphite and on a mesh of 71 values in the range [300,1000] K at 10 K increments for H in H<sub>2</sub>O. A code was written to build the CDFs for beta and alpha at each temperature in the mesh from  $S(\alpha, \beta, T)$  data obtained from NJOY. The  $\beta(T)$  data are then outputted at each  $E_{in}$  and  $P_{\beta}$  in their respective meshes. Likewise, the  $\alpha(T)$  data are outputted at each beta and  $P_{\alpha}$  in their respective meshes. A visualization of this procedure for graphite is shown in Fig. 3 for the beta data and in Fig. 4 for the alpha data. In the figures, only five temperatures (300 K, 650 K, 1000 K, 1500 K and 2000 K) are shown along with four probability lines (0.2, 0.4, 0.6 and 0.8) for one incoming energy value (1 eV) and one beta value (10). This is for visualization purposes only. In actuality, many more temperatures, probability lines, incoming energy values and beta values are used for the study as was described earlier in this section.

Along each CDF probability line, the temperature dependence can be examined through fitting functions. The next section compares different temperature fitting functions to the alpha and beta CDFs for two moderator materials: graphite and H bound in H<sub>2</sub>O.

#### 4. Functional fittings of temperature dependence of alpha and beta for materials of graphite and water

The previous section detailed the procedures for constructing the alpha and beta PDFs/CDFs for each temperature and each

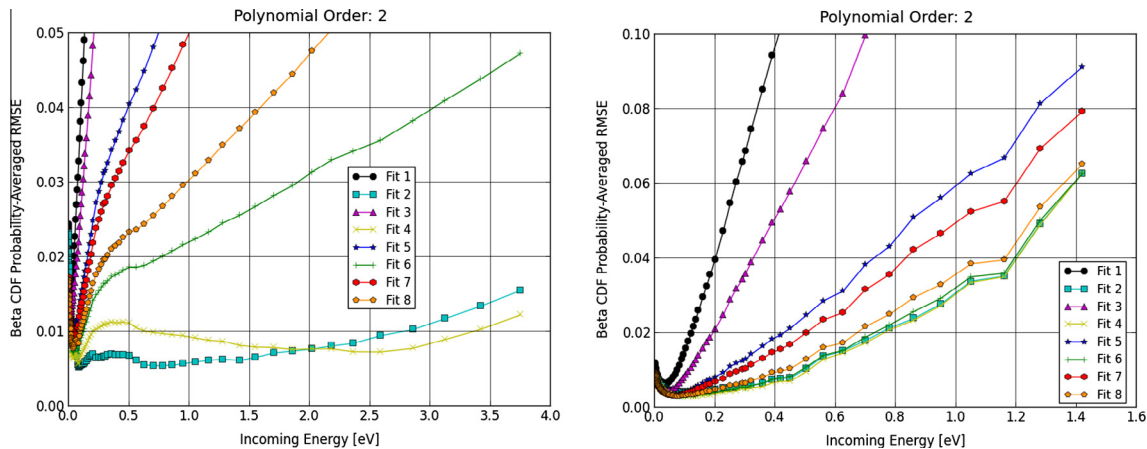


Fig. 5. Beta CDF probability-averaged RMSE as a function of incoming energy for second-order functional expansion fits for graphite (left) and H in H<sub>2</sub>O (right).

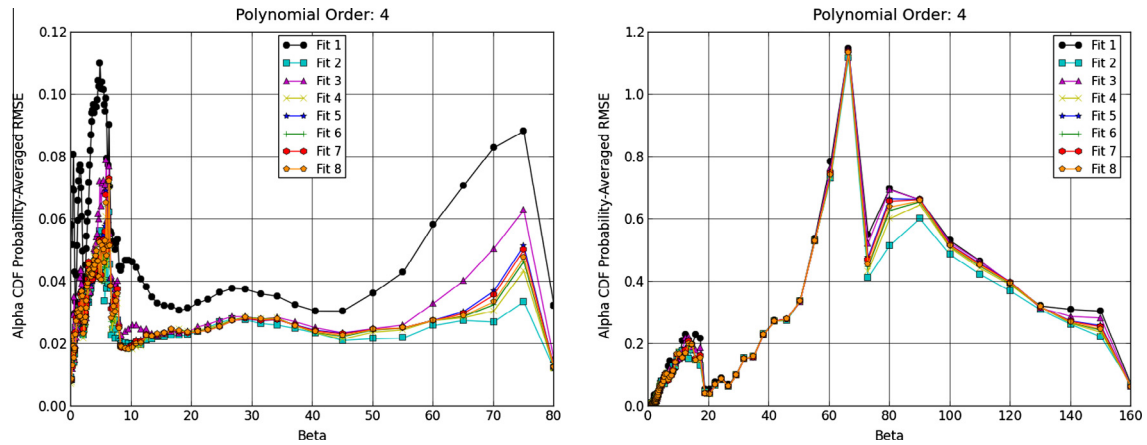


Fig. 6. Alpha CDF probability-averaged RMSE as a function of beta for fourth-order functional expansion fits for graphite (left) and H in H<sub>2</sub>O (right).

Table 5  
Average RMSE for  $\beta(T)$  and  $\alpha(T)$  data for graphite.

Fit #	Beta									
	N = 1	N = 2	N = 3	N = 4	N = 5	N = 6	N = 7	N = 8	N = 9	N = 10
1	0.1198	0.0552	0.0269	0.0135	0.0070	0.0039	0.0024	0.0018	0.0015	0.0014
2	<b>0.0208</b>	0.0059	0.0031	0.0024	0.0020	0.0018	0.0016	0.0015	0.0014	0.0013
3	0.0934	0.0329	0.0119	0.0048	0.0025	0.0018	0.0016	0.0014	0.0014	0.0013
4	0.0421	<b>0.0051</b>	<b>0.0030</b>	0.0023	0.0019	<b>0.0017</b>	0.0015	0.0014	0.0013	<b>0.0013</b>
5	0.0661	0.0154	0.0042	0.0023	<b>0.0019</b>	0.0017	<b>0.0015</b>	0.0014	<b>0.0013</b>	0.0013
6	0.0511	0.0077	0.0030	0.0023	0.0019	0.0017	0.0015	<b>0.0014</b>	0.0013	0.0014
7	0.0622	0.0132	0.0036	<b>0.0023</b>	0.0019	0.0017	0.0015	0.0015	0.0014	0.0014
8	0.0548	0.0093	0.0030	0.0023	0.0019	0.0017	0.0015	0.0015	0.0014	0.0014
Fit #	Alpha									
	N = 1	N = 2	N = 3	N = 4	N = 5	N = 6	N = 7	N = 8	N = 9	N = 10
1	0.1866	0.0986	0.0527	0.0295	0.0185	0.0146	0.0132	0.0121	0.0110	0.0101
2	<b>0.0480</b>	<b>0.0234</b>	<b>0.0175</b>	<b>0.0142</b>	<b>0.0123</b>	<b>0.0107</b>	<b>0.0093</b>	<b>0.0082</b>	<b>0.0073</b>	<b>0.0065</b>
3	0.1571	0.0637	0.0289	0.0174	0.0144	0.0129	0.0118	0.0106	0.0096	0.0086
4	0.0844	0.0241	0.0177	0.0149	0.0127	0.0112	0.0098	0.0087	0.0077	0.0068
5	0.1224	0.0355	0.0192	0.0156	0.0134	0.0120	0.0107	0.0095	0.0084	0.0085
6	0.0997	0.0262	0.0180	0.0153	0.0129	0.0115	0.0102	0.0089	0.0079	0.0080
7	0.1169	0.0324	0.0187	0.0155	0.0133	0.0118	0.0105	0.0106	0.0094	0.0095
8	0.1055	0.0278	0.0182	0.0154	0.0130	0.0116	0.0103	0.0103	0.0091	0.0092

Table 6  
Average RMSE for  $\beta(T)$  and  $\alpha(T)$  data for H in H<sub>2</sub>O.

Fit #	Beta									
	N = 1	N = 2	N = 3	N = 4	N = 5	N = 6	N = 7	N = 8	N = 9	N = 10
1	0.0680	0.0213	0.0073	0.0032	0.0022	0.0019	0.0019	0.0018	0.0018	0.0018
2	<b>0.0104</b>	0.0044	0.0028	0.0022	0.0020	<b>0.0018</b>	0.0018	<b>0.0018</b>	<b>0.0018</b>	<b>0.0017</b>
3	0.0526	0.0122	0.0038	0.0024	0.0020	0.0019	0.0018	0.0018	0.0018	0.0018
4	0.0216	<b>0.0041</b>	<b>0.0028</b>	<b>0.0022</b>	<b>0.0019</b>	0.0018	<b>0.0018</b>	0.0018	0.0018	0.0017
5	0.0370	0.0060	0.0028	0.0022	0.0020	0.0019	0.0018	0.0018	0.0018	0.0018
6	0.0271	0.0042	0.0028	0.0022	0.0020	0.0018	0.0018	0.0018	0.0018	0.0018
7	0.0345	0.0054	0.0028	0.0022	0.0020	0.0019	0.0018	0.0018	0.0018	0.0018
8	0.0295	0.0044	0.0028	0.0022	0.0020	0.0018	0.0018	0.0018	0.0018	0.0018
Fit #	Alpha									
	N = 1	N = 2	N = 3	N = 4	N = 5	N = 6	N = 7	N = 8	N = 9	N = 10
1	0.2539	0.1176	0.0782	0.0651	0.0597	0.0560	0.0523	0.0487	0.0454	0.0426
2	<b>0.1018</b>	<b>0.0790</b>	<b>0.0666</b>	<b>0.0578</b>	<b>0.0516</b>	<b>0.0464</b>	<b>0.0421</b>	<b>0.0391</b>	<b>0.0366</b>	<b>0.0339</b>
3	0.2080	0.0951	0.0708	0.0623	0.0576	0.0536	0.0493	0.0454	0.0420	0.0394
4	0.1215	0.0799	0.0672	0.0592	0.0536	0.0485	0.0438	0.0402	0.0378	0.0357
5	0.1620	0.0833	0.0682	0.0606	0.0557	0.0510	0.0464	0.0424	0.0428	0.0433
6	0.1350	0.0805	0.0675	0.0597	0.0544	0.0494	0.0447	0.0409	0.0411	0.0414
7	0.1550	0.0822	0.0680	0.0604	0.0554	0.0506	0.0459	0.0463	0.0468	0.0472
8	0.1414	0.0809	0.0676	0.0600	0.0547	0.0498	0.0451	0.0454	0.0457	0.0460

incoming energy (or beta) value in its mesh. The temperature dependence of these CDFs is analyzed on appropriately-chosen

CDF probability lines. To determine the best fit for the data, eight different regression models were considered, shown in Table 4.

In Table 4, the  $a_n$ 's are the fitting coefficients and  $N$  is the order of the functional expansion. To determine the best fit for  $\beta(T)$  and  $\alpha(T)$ , the root-mean-square error (RMSE) is calculated at every CDF probability, incoming energy, and beta value. The RMSE is a common measurement used to compare estimated values from a model or functional fit to a true value. The closer RMSE is to zero,

the better the accuracy of the estimated values. The RMSE is given by Frank and Todeschini (1994)

$$RMSE = \sqrt{\frac{\sum_{i=1}^{N_T} (\theta_i - \hat{\theta}_i)^2}{N_T - (N + 1)}} \tag{28}$$

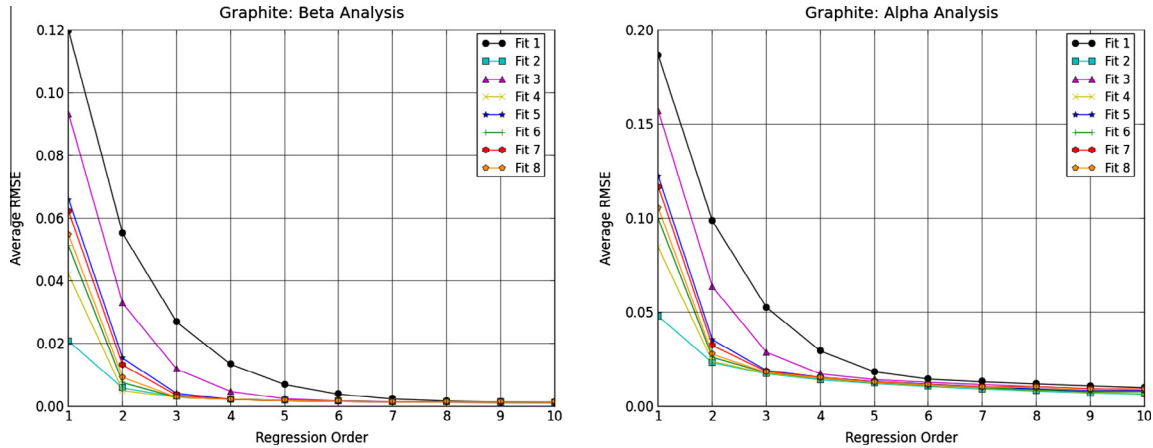


Fig. 7. Regression order vs. Average RMSE for graphite, left: beta data, right: alpha data.

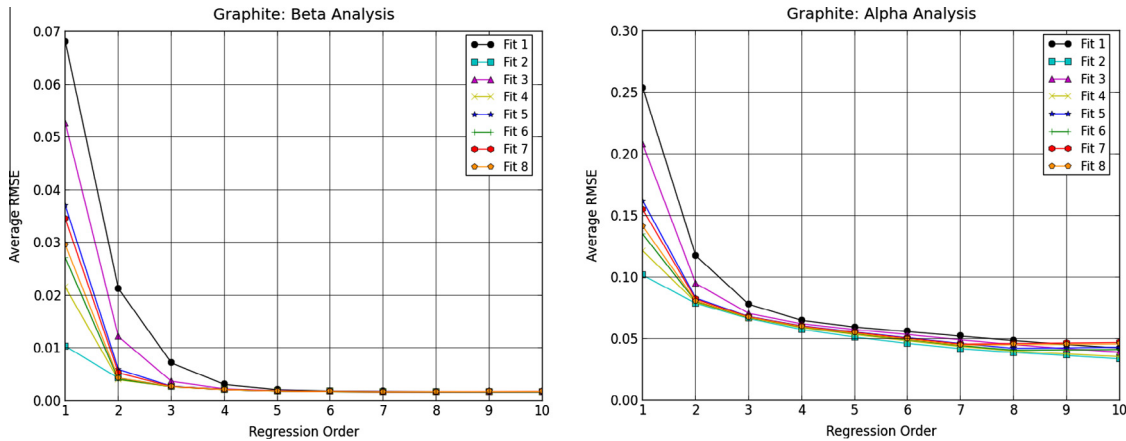


Fig. 8. Regression order vs. Average RMSE for H in H<sub>2</sub>O, left: beta data, right: alpha data.

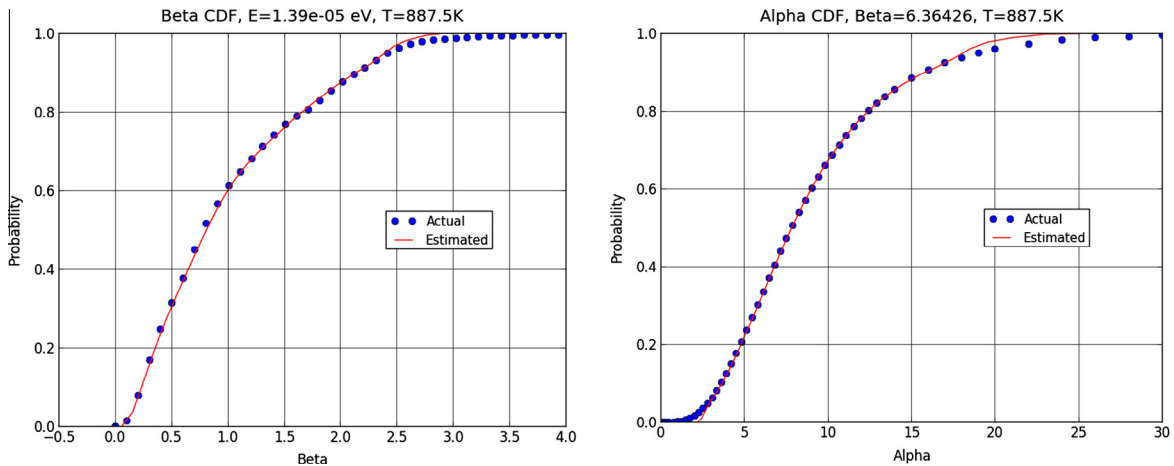


Fig. 9. Comparison of estimated and true CDFs for graphite,  $T = 887.5$  K. Left: beta CDF,  $E_{in} = 1.39E-5$  eV, right: alpha CDF,  $\beta = 6.36426$ .

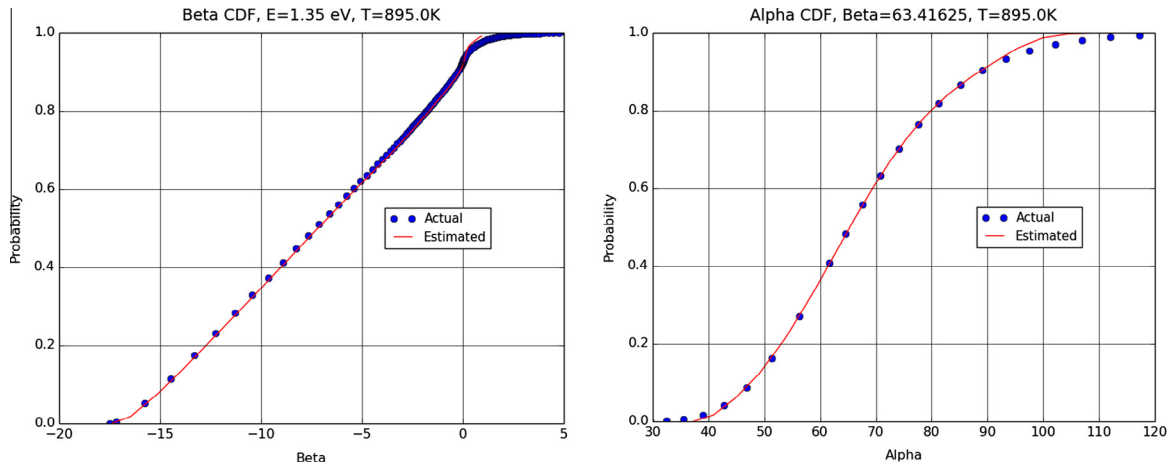


Fig. 10. Comparison of estimated and true CDFs for H in H<sub>2</sub>O, T = 895 K. Left: beta CDF,  $E_{in} = 1.35$  eV, right: alpha CDF,  $\beta = 63.41625$ .

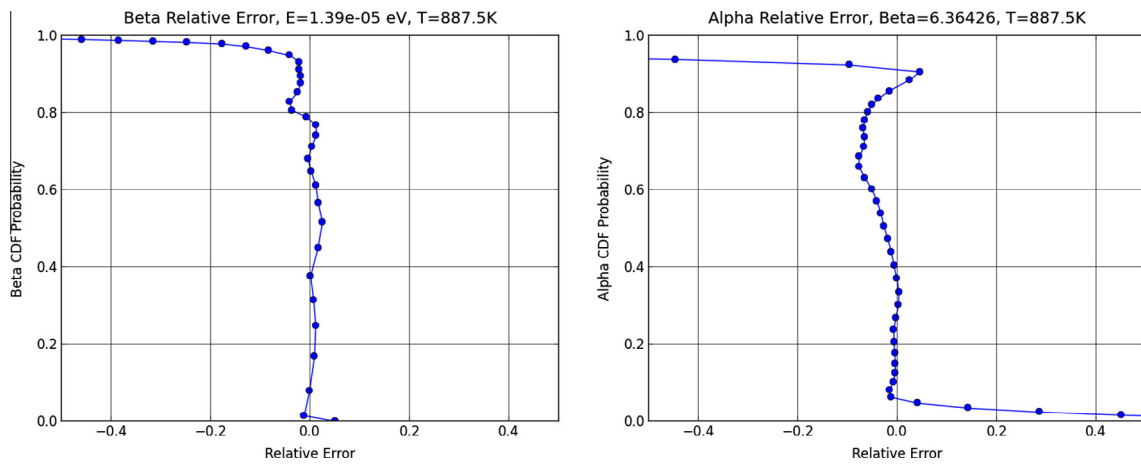


Fig. 11. Relative error between estimated and true beta (left) and alpha (right) for graphite, Left: beta CDF,  $E_{in} = 1.39E-5$  eV,  $T = 887.5$  K, right: alpha CDF,  $\beta = 6.36426$ ,  $T = 887.5$  K.

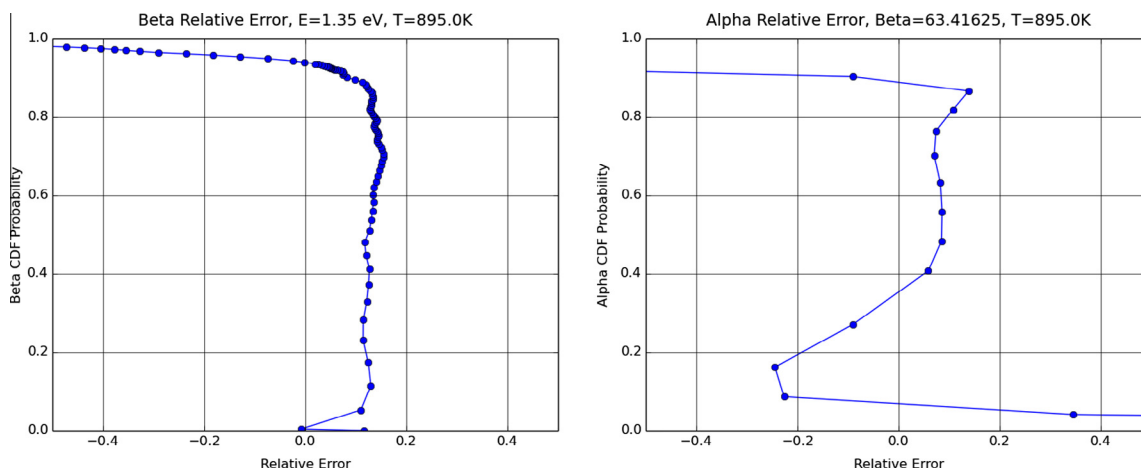


Fig. 12. Relative error between estimated and true beta (left) and alpha (right) for H in H<sub>2</sub>O, Left: beta CDF,  $E_{in} = 1.35$  eV,  $T = 895$  K, right: alpha CDF,  $\beta = 63.41625$ ,  $T = 895$  K.

Table 7  
Fitting coefficient testing: mesh points used for graphite and water.

Incoming Energy [eV]		Beta		Temperature [K]	
Graphite	Water	Graphite	Water	Graphite	Water
0.0044	0.0008	1.4252	8.5899	378.08	406.97
0.0743	0.0267	35.7380	32.1844	809.61	681.82
0.3719	0.0858	55.3908	72.6508	1057.46	793.70
1.1929	0.2993	65.7804	110.4076	1506.88	851.48
3.4937	0.8021	74.4940	147.1760	1919.13	920.36

where  $\theta_i$  is the true value of beta or alpha at the current temperature,  $\hat{\theta}_i$  is the estimated value of beta or alpha at the current temperature from the fitting coefficients and  $N_T$  is the number of temperature values used in the analysis. The true value of beta and alpha is found by running the LEAPR module of NJOY at the desired temperature to obtain the  $S(\alpha, \beta, T)$  data. In addition to the temperature, LEAPR requires a uniform energy transfer grid along with values of the phonon frequency spectrum at each energy transfer. An appropriate alpha/beta grid must also be input. Then, Eqs. (14) and (18) are used to build the true PDFs. These RMSE

values are then averaged over the 39 CDF probability lines. Fig. 5 shows the probability-averaged RMSE for each fit as a function of the incoming energy mesh for a second-order functional expansion for the  $\beta(T)$  data for graphite (left) and H in H<sub>2</sub>O (right). A second-order functional expansion is shown as an example. However, orders from one to ten were examined in the study.

Fig. 6 shows the probability-averaged RMSE for each fit as a function of the beta mesh for a fourth-order functional expansion

fit for the  $\alpha(T)$  data for graphite (left) and H in H<sub>2</sub>O (right). A fourth-order functional expansion is shown as an example. However, orders from one to ten were examined in the study.

From Figs. 5 and 6, there is a lot of fluctuation in the probability-averaged RMSE over the entire incoming energy and beta meshes. It was decided to average these values to obtain one RMSE value for each fit. Tables 5 and 6 show these averaged RMSE for the  $\beta(T)$  and  $\alpha(T)$  data for functional expansion orders

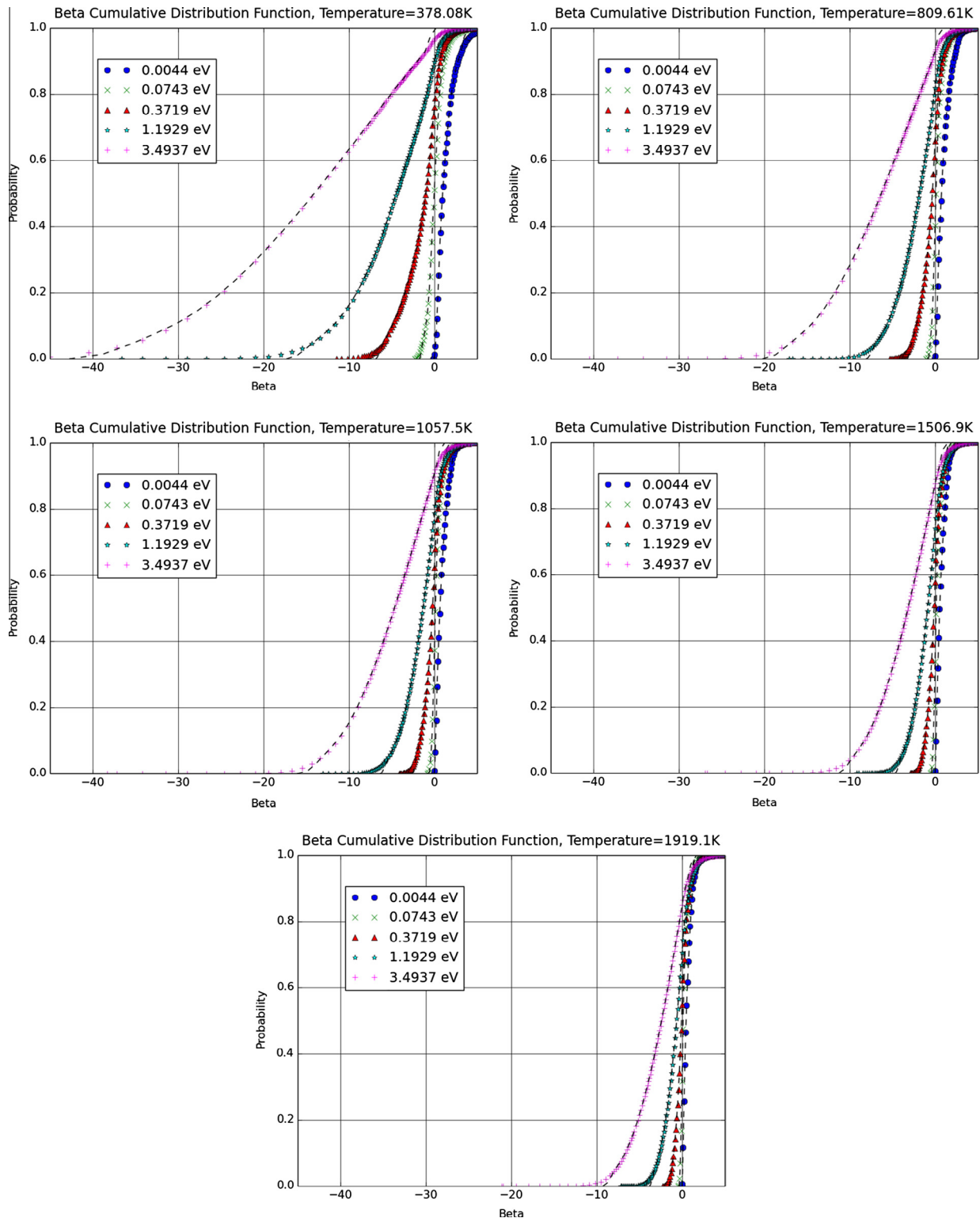


Fig. 13. Comparison of estimated and true beta CDFs for graphite for various temperatures and incoming neutron energies.

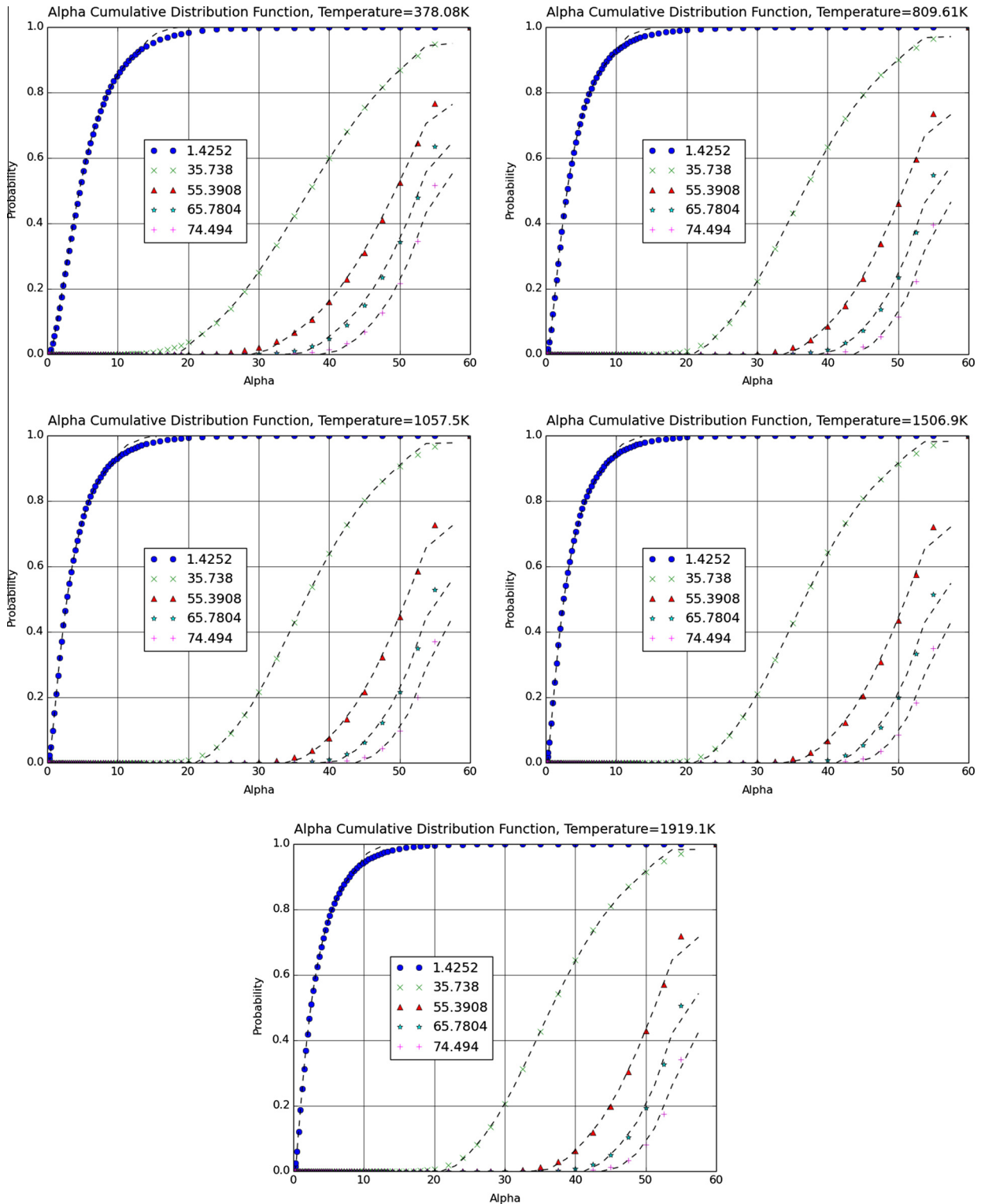


Fig. 14. Comparison of estimated and true alpha CDFs for graphite for various temperatures and beta values.

one through ten for graphite and H in H<sub>2</sub>O, respectively. The lowest RMSE for a particular functional expansion order is bolded.

The best fit is the one with the lowest average RMSE. As the order of the functional expansion increases, the average RMSE decreases, but the storage of more coefficients is necessary. To determine which order is best to use, the change in the average RMSE between adjacent functional expansion orders for a specific

fit should be small. The order of the regression model versus the average RMSE in Fig. 7 and for H in H<sub>2</sub>O in Fig. 8.

From Tables 5 and 6 and Figs. 7 and 8,  $\sum_{n=0}^2 a_n (\sqrt{T})^{-n}$  (Fit 4) is chosen for the  $\beta(T)$  data over the entire incoming energy mesh for both graphite and H in H<sub>2</sub>O (with averaged RMSE of 0.0051 and 0.0041, respectively). Likewise,  $\sum_n = 0^4 a_n T^{-n}$  (Fit 2) is chosen for the  $\alpha(T)$  data over the entire beta mesh for both graphite and H

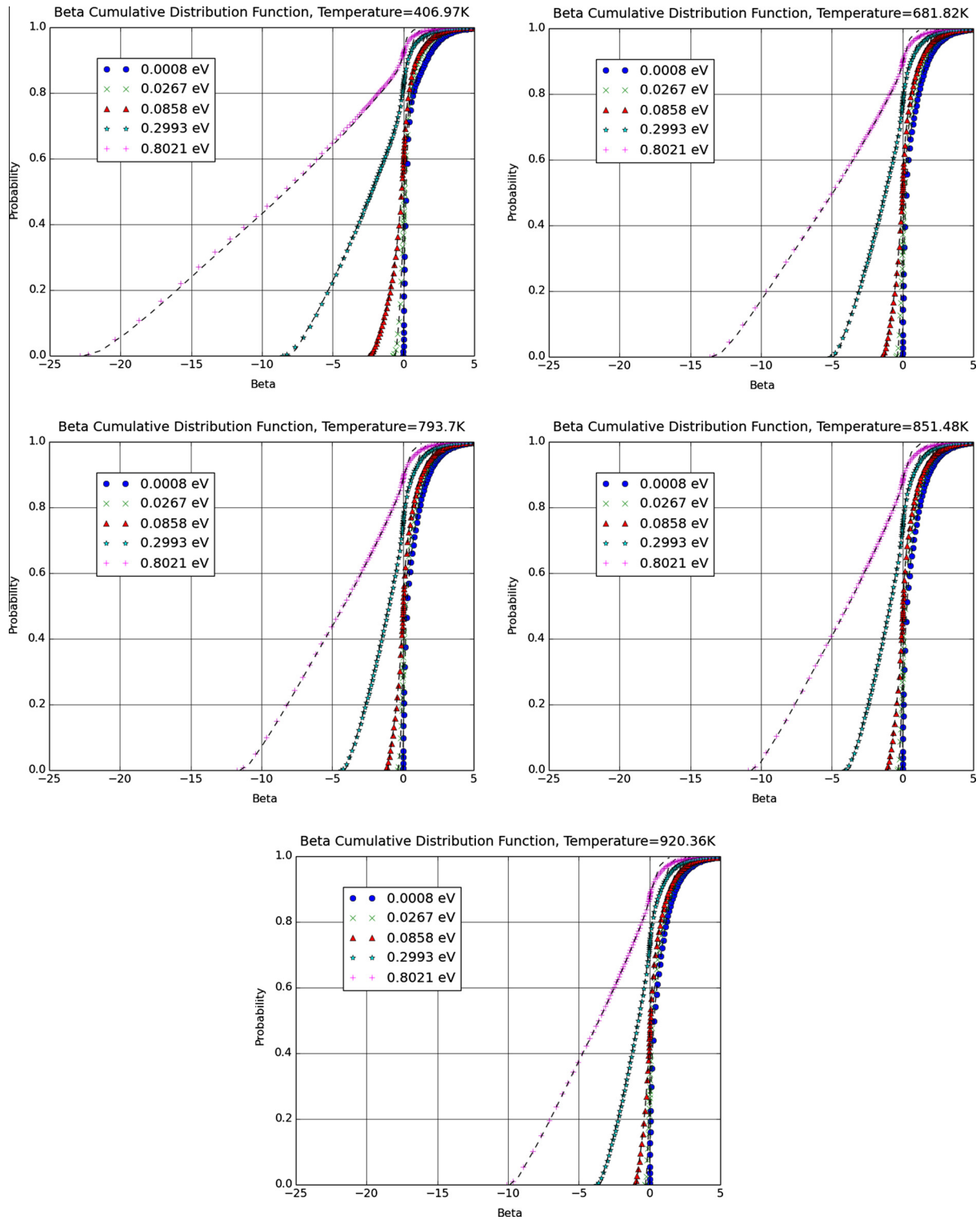


Fig. 15. Comparison of estimated and true beta CDFs for H in H<sub>2</sub>O for various temperatures and incoming neutron energies.

in H<sub>2</sub>O (with averaged RMSE of 0.0142 and 0.0578, respectively). The beta coefficient files for graphite and H in H<sub>2</sub>O have a total storage of 190 kB and 168 kB, respectively. The alpha coefficient files for graphite and H in H<sub>2</sub>O have a total storage of 271 kB and 272 kB, respectively. In total, the coefficient files for graphite and H in H<sub>2</sub>O only require 461 kB and 440 kB, respectively. Storing coefficients is beneficial because they can be used to sample outgoing energy and cosine of the scattering angle for any temperature and any incoming neutron energy.

### 5. Sampling testing based on fitted functional expansions

The beta coefficients are stored at discrete CDF probability values and at discrete incoming energies. Similarly, the alpha coefficients are stored at discrete CDF probability values and at discrete beta values. Of course, in actual sampling, values of  $E_{in}$ , beta and CDF probability are encountered that the coefficients are not stored for. When this occurs, linear interpolation is performed between sets to the desired value.

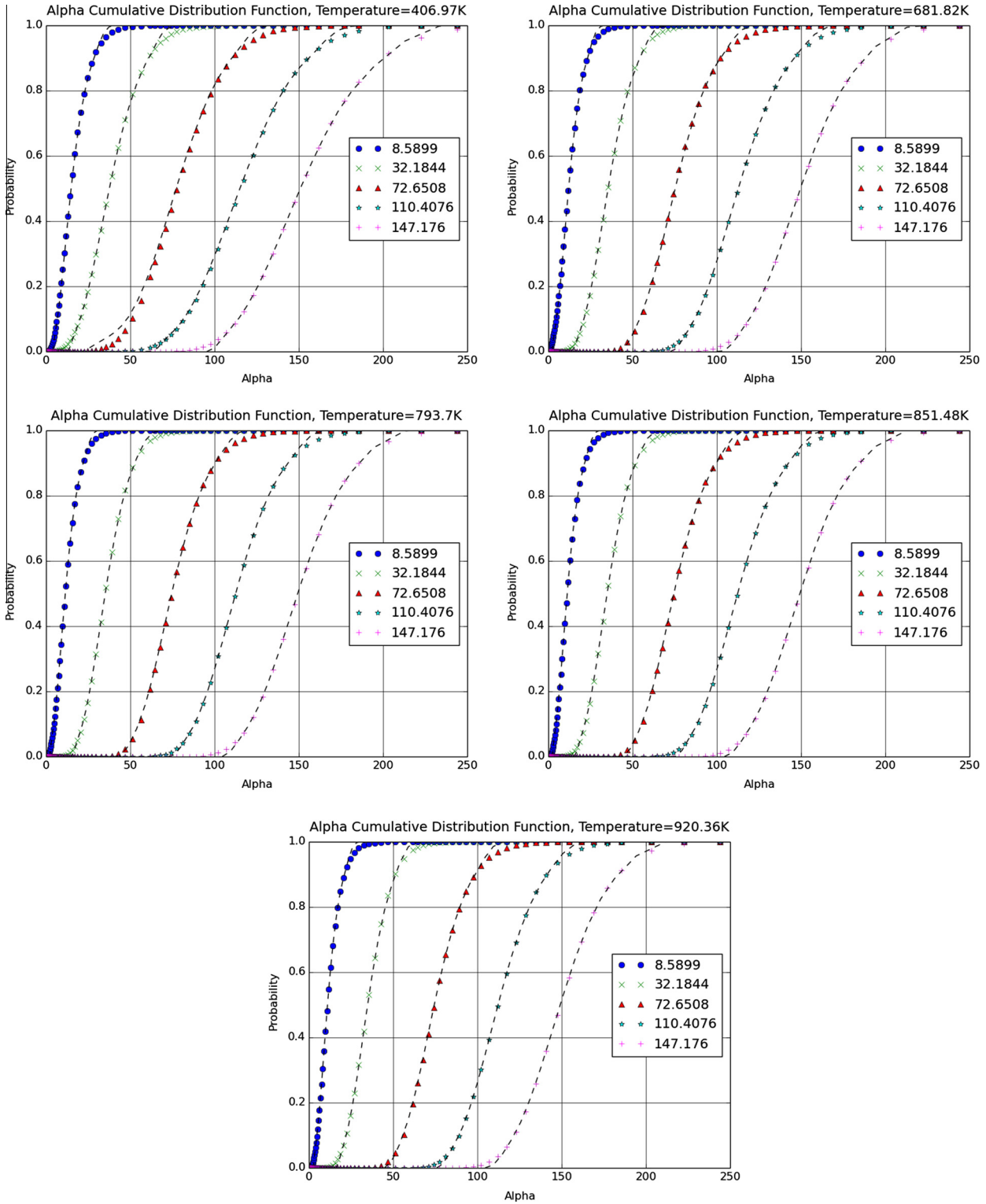


Fig. 16. Comparison of estimated and true alpha CDFs for H in H<sub>2</sub>O for various temperatures and beta values.

To sample alpha and beta from the coefficients given an incoming neutron energy and temperature, the beta coefficient file is searched for the two closest incoming energy sets,  $E_1$  and  $E_2$  such that  $E_1 < E_{in} < E_2$ . Then, a uniform pseudorandom number,  $\xi_1$ , in  $[0, 1]$  is sampled and the beta coefficient file is searched for the two closest CDF probability sets,  $P_{\beta 1}$  and  $P_{\beta 2}$  such that  $P_{\beta 1} < \xi_1 < P_{\beta 2}$ . At these four sets ( $E_1$ ,  $E_2$ ,  $P_{\beta 1}$  and  $P_{\beta 2}$ ), the temperature and the coefficients in these sets are used to calculate a value of beta. Then,

linear interpolation is done to the true  $E_{in}$  and  $\xi_1$ . From this sampled beta value ( $\beta_s$ ), the alpha coefficient file is searched for the two closest beta sets  $\beta_1$  and  $\beta_2$  such that  $\beta_1 < \beta_s < \beta_2$ . Then, another uniform pseudorandom number,  $\xi_2$ , in  $[0, 1]$  is sampled and the alpha coefficient file is searched for the two closest CDF probability sets  $P_{\alpha 1}$  and  $P_{\alpha 2}$  such that  $P_{\alpha 1} < \xi_2 < P_{\alpha 2}$ . Like before, linear interpolation is performed between the sets to determine the sampled value of alpha.

To test the goodness of these coefficients, a simple Monte Carlo code was written to sample alpha and beta many times using only the coefficient files. The ranges of possible alpha and beta values were each divided into equally spaced bins,  $\Delta t$ . For example, the beta range for graphite extends from  $-80$  to  $80$ . This range was divided into 1600 equally-spaced bins of width  $\Delta t = 0.1$ , while the beta range for H in  $H_2O$  extends from  $-160$  to  $160$  and was divided into 1600 equally-spaced bins of width  $\Delta t = 0.2$ . The alpha range for graphite extends from  $0$  to  $60$ . This range was also divided into 1600 equally-spaced bins of width  $\Delta t = 0.0375$ , while the alpha range for H in  $H_2O$  extends from  $0$  to  $321.29$  and was divided into 1600 equally-spaced bins of width  $\Delta t = 0.201$ . The relative frequency of each sample is determined by

$$f_i = \frac{N_i}{N\Delta t}, \quad (29)$$

where  $N_i$  is the number of samples that fall into bin  $i$ . As the number of samples run in the Monte Carlo code increases, a plot of the mid-point of each bin versus the relative frequency approaches the true PDF. Integrating over this produces the CDF.

To test the beta coefficients, it was decided to choose an incoming energy not contained in the coefficient file. Since linear interpolation is performed between energy sets to the true incoming energy, it is best to choose an incoming energy that is halfway between two adjacent energy sets to test the effectiveness of the linear interpolation. Also, the incoming energy chosen should be such that its two adjacent energy sets have the largest RMSE for the chosen fit (to test the goodness of the coefficients).

For graphite, from Fig. 5 for Fit 4, the largest average RMSE occurs for  $E_1 = 1E-5$  eV and  $E_2 = 1.78E-5$  eV. The energy halfway between these two values is chosen for the analysis,  $E_{in} = 1.39E-5$  eV. A similar approach is taken to test the alpha coefficients. The largest average RMSE occurs for  $\beta_1 = 6.28855$  and  $\beta_2 = 6.43997$ . The beta value halfway between these two values is chosen for the analysis,  $\beta = 6.36426$ . Finally, a temperature of  $887.5$  K is chosen since the coefficients were determined at discrete temperatures, two of which include  $875$  K and  $900$  K. The value of  $887.5$  K is halfway between these temperatures.

For H in  $H_2O$ , from Fig. 5 for Fit 4, the largest average RMSE occurs for  $E_1 = 1.28$  eV and  $E_2 = 1.42$  eV. The energy halfway between these two values is chosen for the analysis,  $E_{in} = 1.35$  eV. For the alpha coefficients, the largest average RMSE occurs for  $\beta_1 = 60.4771$  and  $\beta_2 = 66.3554$ . The beta halfway between these two values is chosen for the analysis,  $\beta = 63.41625$ . Finally, a temperature of  $895$  K is chosen, which is halfway between the temperatures  $890$  K and  $900$  K (two of the temperatures used to determine the fitting coefficients).

Figs. 9 and 10 compare the estimated beta CDF (left) and alpha CDF (right) for graphite and H in  $H_2O$ , respectively, found from the fitting coefficients to the true beta and alpha CDF, respectively, calculated from the true  $S(\alpha, \beta, T)$  data and constructed using Eqs. (16) and (19).

The largest relative errors occur for very high CDF probability values as shown in Figs. 11 and 12. This is because the smallest and largest CDF probability lines chosen for the temperature analysis are  $0.025$  and  $0.975$  and the true CDF data has many beta/alpha values at CDF values between  $0$  and  $0.025$  as well as between  $0.975$  and  $1.0$ . The standard deviation for the number of sampled values that fall inside these bins is quite large, resulting in the large relative errors. If the number of samples run is increased sufficiently, more of the sampled values will fall into these bins and better agreement will be observed. For graphite, the largest relative errors in the majority of the CDF region,  $[0.025, 0.9]$  is  $0.029$  for beta and  $0.141$  for alpha. For water, the largest relative errors in this CDF region are  $0.155$  for beta and  $0.346$  for alpha.

Next, the effectiveness of the fitting coefficients is shown over the range of incoming neutron energies, beta values and temperatures. Uniform random mesh points were chosen for both graphite and water and the coefficients were tested at these values. Table 7 shows the chosen parameters for graphite and water.

The beta CDFs were tested using the temperatures and incoming energies listed in Table 7 while the alpha CDFs were tested using the temperatures and beta values listed in the table. Figs. 13 and 14 compare the estimated beta and alpha CDFs, respectively, for graphite found from the fitting coefficients to the true CDFs calculated from the true  $S(\alpha, \beta, T)$  data. Figs. 15 and 16 show the comparison for H in  $H_2O$ . In these figures, the dotted lines represent the estimated CDF from the fitting coefficients while the markers represent the true CDF data.

These results show that the fitting coefficients can accurately reproduce the alpha and beta CDFs even for the most sensitive values of energy, beta and temperature. Some discrepancy is observed at very low and very high CDF probability values, indicating that more probability lines should be used. Therefore, these fitting coefficients are suitable to sample outgoing energy and cosine of the scattering angle for graphite for any thermal energy and any temperature.

## 6. Conclusions

On-the-fly sampling methods have been developed in recent years to reduce the storage of cross section data for Monte Carlo simulations. For the most important resonance absorber nuclides, an on-the-fly Doppler broadening method has been developed to obtain the cross section at the desired temperature and incoming energy from pre-stored zero-temperature cross section data and appropriate functional expansions. A stochastic method accounting for the thermal motion of target nuclei on-the-fly has also recently been implemented into the Monte Carlo code Serpent. In the epithermal energy range, both the DBRC method and WCM have been developed to on-the-fly sample a neutron's outgoing energy and angle after a scattering reaction in the center-of-mass frame. More recently, a method has been developed to on-the-fly generate the moments of the differential scattering PDF for any temperature in the laboratory frame.

These methods are not applicable for thermal inelastic neutron scattering data due to the complicated nature of chemical and binding effects at low neutron energies. To address this, PDFs and CDFs of energy and momentum transfer were constructed from the methods of Ballinger and the temperature dependence of these CDFs was examined along lines of equal probability. For the beta CDF, second-order functional expansions with the regression model using  $1/\sqrt{T}$  as the basis provided the best fit for the temperature dependence over the incoming energy mesh with an averaged RMSE of  $0.0051$  for graphite and  $0.0041$  for H in  $H_2O$ . For the alpha CDF, fourth-order functional expansions in  $1/T$  provided the best fit for the temperature dependence over the beta mesh with an averaged RMSE of  $0.0142$  for graphite and  $0.0578$  for H in  $H_2O$ .

Sampling from the coefficients of these functional expansions was tested with a simple Monte Carlo code for the values of incoming energy and beta that were most sensitive to the chosen fits. It was shown that these coefficients can accurately sample values of the energy and momentum transfer for graphite with only minor errors. These observed errors in the sampled values have not yet been tested on reactor parameters like reaction rates, k-effective, etc. A future study will test the effectiveness of these coefficients in the thermal range in a realistic Monte Carlo problem. The total storage space of all coefficients is  $461$  kB for graphite and  $440$  kB for H in  $H_2O$  and can be used to sample outgoing energy and angle for any incoming energy and any temperature. This is a significant improvement of the current method which requires around  $24$  MB

of storage *per temperature*. The coefficients are more compact than the current ACE data and can be combined with the on-the-fly Doppler broadening scheme in the future to complete the modeling of temperature effects for Monte Carlo codes.

## Acknowledgments

This work is supported by the RPI-NRC Nuclear Fellowship Program under the grant NRC-38-10-950. The authors thank Dr. Timothy Trumbull of Knolls Atomic Power Laboratory, Dr. Forrest Brown and Dr. Brian Kiedrowski of Los Alamos National Laboratory and Professor William Martin of the University of Michigan for their assistance and guidance with this work. The authors also thank Ms. Megan Wart for her efforts in helping to write the script to read the ENDF library data.

## References

- Ballinger, C.T., 1995. The Direct  $S(\alpha, \beta)$  Method for Thermal Neutron Scattering. Proc. of the International Conference on Mathematics and Computation, Reactor Physics, and Environmental Analysis, 1, 134. Portland, Oregon.
- Becker, B., Dagan, R., Lohnert, G., 2009. Proof and implementation of the stochastic formula for ideal gas, energy dependent scattering kernel. *Ann. Nucl. Energy* 36, 470–474.
- Bischoff, F.G., Yeater, M.L., 1972. Monte Carlo evaluation of multiple scattering and resolution effects in double-differential neutron scattering cross-section measurements. *Nucl. Sci. Eng.* 48, 266–280.
- Brown, F.B., Martin, W.R., Yesilyurt, G., Wilderman, S., 2012. On-the-Fly Neutron Doppler Broadening for MCNP. Los Alamos National Laboratory. Report LA-UR-12-00700.
- Carter, L.L., Cashwell, E.D., 1975. Particle transport simulation with the monte carlo method. TI D-26607. Los Alamos National Laboratory.
- CSEWG, 2011. ENDF-6 Formats Manual. Brookhaven National Laboratory Report BNL-90365-2009 Rev. 2.
- Frank, I.E., Todeschini, R., 1994. *The Data Analysis Handbook (Data Handling in Science and Technology)*. Elsevier Science.
- Koppel, J.U., Triplett, J.R., Naliboff, Y.D., 1967. GASKET—A Unified Code for Thermal Neutron Scattering. General Atomic Division of General Dynamics Report GA-7417.
- Lee, D., Smith, K., Rhodes, J., 2009. The impact of U-238 resonance elastic scattering approximations on thermal reactor Doppler reactivity. *Ann. Nucl. Energy* 36, 274–280.
- MacFarlane, R.E., Muir, D.W., Boicourt, R.M., Kahler, A.C., 2012. The NJOY Nuclear Data Processing System, Version 2013. Los Alamos National Laboratory Report LA-UR-12-27079.
- Pavlou, A.T., Brown, F.B., Martin, W.R., Kiedrowski, B.C., 2012. Comparison of discrete and continuous thermal neutron scattering treatments in MCNP5. In: Proc. of PHYSOR 2012 – Advances in Reactor Physics, Knoxville, Tennessee.
- Sunny, E.E., Martin, W.R., 2013. On-the-fly generation of differential resonance scattering probability distribution functions for Monte Carlo codes. In: Proc. of the International Conference on Mathematics and Computational Methods Applied to Nuclear Science & Engineering (M&C 2013), Sun Valley, Idaho.
- Sutton, T.M., Donovan, T.J., Trumbull, T.H., Dobreff, P.S., Caro, E., Griesheimer, D.P., Tyburski, L.J., Carpenter, D.D., Joo, H., 2007. The MC21 Monte Carlo transport code. In: Proc. of the Joint International Topical Meeting on Mathematics & Computation and Supercomputing in Nuclear Applications (M&C + SNA 2007), Monterey, California.
- Sutton, T.M., Trumbull, T.H., Lubitz, C.R., 2009. Comparison of some Monte Carlo models for bound hydrogen scattering. In: Proc. of the International Conference on Mathematics and Computational Methods Applied to Nuclear Science & Engineering (M&C 2009), Saratoga Springs, New York.
- Terrani, K.A., 2012. Incorporation of Hydride Nuclear Fuels in Commercial Light Water Reactors. University of California, Berkley Doctoral Dissertation.
- Viitanen, T., Leppänen, J., 2012. Explicit treatment of thermal motion in continuous-energy Monte Carlo tracking routines. *Nucl. Sci. Eng.* 171, 165–173.
- Vilim, R.B., Feldman, E.E., Pointer, W.D., Wei, T.Y.C., 2004. Initial VHTR Accident Scenario Classification: Models and Data. Argonne National Laboratory, Nuclear Engineering Division Status Report ANL-GenIV-057.
- Goorley, T., James, M., Booth, T., Brown, F., Bull, J., Cox, L.J., Durkee, J., Elson, J., Fensin, M., Forster, R.A., Hendricks, J., Hughes, H.G., Johns, R., Kiedrowski, B., Martz, R., Mashnik, S., McKinney, G., Pelowitz, D., Prael, R., Sweezy, J., Waters, L., Wilcox, T., Zukaitis, T., 2012. Initial MCNP 6 Release Overview. Los Alamos National Laboratory Report LA-UR-11-07082. *Nucl. Tech.* 180, 298–315.
- Yesilyurt, G., Ji, W., Prasad, S., Martin, W.R., Lee, J.C., 2007. Coupled nuclear-thermal-hydraulics analysis for VHTR. *Trans. Am. Nucl. Soc.* 96, 580–581.
- Yesilyurt, G., Martin, W.R., Brown, F.B., 2012. On-the-fly Doppler broadening for Monte Carlo codes. *Nucl. Sci. Eng.* 171, 239–257.